

Available online at www.sciencedirect.com

ScienceDirect

www.elsevier.com/locate/jes

JES
JOURNAL OF
ENVIRONMENTAL
SCIENCES
www.jesc.ac.cn

Highly efficient Hg^{2+} removal via a competitive strategy using a Co-based metal organic framework ZIF-67

Jiacheng Zhou¹, Hao Zhang¹, Tianying Xie¹, Ye Liu¹, Qicheng Shen¹,
Jie Yang¹, Limei Cao^{1,2,*}, Ji Yang^{1,2,*}

¹ School of Resources and Environmental Engineering, State Environmental Protection Key Laboratory of Environmental Risk Assessment and Control on Chemical Process, East China University of Science and Technology, Shanghai 200237, China

² Shanghai Institute of Pollution Control and Ecological Security, Shanghai 200092, China

ARTICLE INFO

Article history:

Received 18 May 2021

Revised 6 August 2021

Accepted 17 August 2021

Available online 14 January 2022

Keywords:

ZIF-67

Hg^{2+} removal

Coordination competition

ABSTRACT

The stronger coordination ability of mercury ions with organic ligands than the metal ions in metal organic framework (MOFs) provides an accessible way to separate mercury ions from solution using specific MOFs. In this study, a Co-based MOF (ZIF-67, $\text{Co}(\text{mIM})_2$) was synthesized. It did not introduce specific functional groups, such as $-\text{SH}$ and $-\text{NH}_2$, into its structure through complicated steps. It separate Hg^{2+} from wastewater with a new strategy, which utilized the stronger coordination ability of Hg^{2+} with the nitrogen atom on the imidazole ring of the organic ligand than the Co^{2+} ions. Hg^{2+} replaced Co^{2+} nodes from ZIF-67 and formed a more stable precipitate with mIM. The experimental results showed that this new strategy was efficient. ZIF-67 exhibited Hg^{2+} adsorption capacity of 1740 mg/g, much higher than the known MOFs sorbents. mIMs is the reaction center and ZIF-67 can improve its utilization. The sample color faded from purple to white due to the loss of cobalt ion. It is a great feature of ZIF-67 that allows users to judge whether the sorbent is deactivated intuitively. ZIF-67 can be sustainable recycled by adding organic ligands to the solution after treatment due to its simple synthesis method at room temperature. It's a high-efficient and sustainable sorbent for Hg^{2+} separation from wastewater.

© 2022 The Research Center for Eco-Environmental Sciences, Chinese Academy of Sciences. Published by Elsevier B.V.

Introduction

The increasing anthropogenic emissions of mercury to water bodies, deriving from oil refinery, pesticide, Chlor-alkali, dyestuff, battery manufacturing, and metal smelting industry have been considered a considerable threat to the ecological environment and human health worldwide (Krishnan and

Anirudhan, 2002; Wang et al., 2010; Xia et al., 2019). The major health effects of mercury poisoning as a result of exposure are of a longer-term, leading to neurological and renal disturbances (Jeon and Park, 2005; Olson et al., 2000). It must be emphasized that a high concentration of mercury during pregnancy is a serious problem that Hg^{2+} can easily pass the blood-brain barrier and affect the fetal brain (Li et al., 2020).

To control the increasingly serious mercury pollution, various materials were studied on the subject of mercury removal from wastewater. TMT-55 (2,4,6-Trimercaptotriazine, a

* Corresponding authors.

E-mails: caolimei@ecust.deu.cn (L. Cao), yangji@ecust.edu.cn (J. Yang).

Table 1 – An overview of the parameters and Hg²⁺ removal performance of various MOFs sorbents.

MOF	Hg ²⁺ source	Optimal pH	Adsorption capacity (mg/g)	Equilibrium time (min)	Refs.
Cu-BTC-DGT	HgCl ₂	-	714	120	(Ke et al., 2011a)
FJI-H12	HgCl ₂	7	440	60	(Liang et al., 2016)
UiO-66-SH	Hg(NO ₃) ₂	-	243	-	(Yee et al., 2013)
[Ni(3-bpd) ₂ (NCS) ₂] _n	Hg(NO ₃) ₂	-	713	120	(Halder et al., 2017)
ZIF-90-SH	HgCl ₂	-	22	-	(Bhattacharjee et al., 2015)
Zn(hip)(L)•(DMF)(H ₂ O)	HgCl ₂	5	278	60	(Luo et al., 2015)
ZIF-67	HgCl ₂	4	1740	120	this study

trisodium salt nonahydrate) can chemically precipitate most heavy metal ions, including Hg²⁺, through sulfur groups (Matlock et al., 2001). Activated carbon is widely used as an adsorbent in treating wastewater due to its highly porous structure and rich functional groups (Babic et al., 2002; Liu et al., 2018). Among several chemical activations, ZnCl₂ activated carbon exhibited the highest Hg²⁺ adsorption capacity of 152 mg/g (Zabihi et al., 2010; Zhang et al., 2005). As a porous material, silica did not perform as well as other adsorbents for mercury removal, but its easier functionalization made it widely studied for mercury removal (Choi et al., 2016; Song et al., 2011). Phosphinic acid-functionalized silica demonstrated excellent Hg²⁺ adsorption efficiency of 99.11%, and its maximum adsorption capacity was up to 274 mg/g (Xiong et al., 2018). Chitosan could use the amine groups on its surface to capture mercury ions. The high mercury adsorption capacity of 435 mg/g and reproducibility made aminated chitosan a promising adsorbent (Jeon and Park, 2005). These materials performed well in removing Hg²⁺ from wastewater. However, the desire for more efficient, low-cost, and renewable sorbents drives the search for new materials.

Recently, metal-organic frameworks (MOFs), a new class of porous solid materials, have been developed as mercury sorbents for wastewater treatment due to their rich pore structure and easy functionalization (Zhao et al., 2018; Zou et al., 2013). By choosing different metal ions and organic ligands, MOFs with different structures and functions can be constructed (Liu et al., 2019b). Introducing target groups into MOFs by functionalizing the organic ligands is a common strategy to transform MOFs into Hg²⁺ sorbents. Sulfur groups are useful for mercury uptake (Ramezani et al., 2020). Many studies have been carried on applying thiol-functionalized MOFs to the separation of Hg²⁺. They introduced sulfur-containing groups to the benzene ring of the organic ligand and their great mercury adsorption performance had been confirmed, as shown in Table 1 (Bhattacharjee et al., 2015; Halder et al., 2017; Ke et al., 2011a; Liang et al., 2016; Yee et al., 2013). Nitrogen-containing groups can fix metal ions, such as Pt²⁺, Hg²⁺, Pd²⁺ and so on (Saleem et al., 2016; Wang et al., 2019). A novel MOF adsorbent Zn(hip)(L)•(DMF)(H₂O) reported by (Luo et al., 2015) performed high mercury adsorption capacity, and it captured mercury ions through the free hydroxyl and acylamide groups in the channels.

In this study, ZIF-67 was synthesized, which is a kind of zeolitic imidazolate frameworks (ZIFs) with exceptional chemical and thermal stability (Park et al., 2006). In ZIF-67, transi-

tion metal ions (Co²⁺) formed bonds with the N atoms of 2-methylimidazole (mIM), and the Co-mIM-Co angle was near 145°, which was coincident with the Si-O-Si angle found in many zeolites (Banerjee et al., 2008). It has a porous structure and huge specific surface area.

ZIF-67 does not introduce specific functional groups into its structure through complicated steps because it does not capture Hg²⁺ through functional groups, which is different from the MOFs sorbents mentioned above. It separate Hg²⁺ from wastewater with a new strategy, which utilized the stronger coordination ability of Hg²⁺ with organic ligand than the Co²⁺ ions in ZIF-67. Hg²⁺ replaced Co²⁺ nodes from ZIF-67 and formed a more stable precipitate with mIM. The experimental results showed that this new strategy is more efficient than MOFs functionalization. ZIF-67 exhibited a huge Hg²⁺ adsorption capacity of 1740 mg/g, much higher than the known MOFs sorbents, as shown in Table 1. Moreover, ZIF-67 can be sustainable recycled by adding organic ligands to the solution after treatment due to its simple synthesis method at room temperature. It's a high-efficient and sustainable sorbent for Hg²⁺ removal from wastewater.

1. Experimental

1.1. Sorbent preparation

In a typical synthesis of ZIF-67, 0.2913 g Co(NO₃)₂•6H₂O (AR, ≥99%, Aladdin Chemistry Co., Ltd.) and 0.3284 g 2-mIM (98%, Macklin Biochemical Co., Ltd.) were dissolved in 25 mL of methanol (AR, ≥99.5%, Aladdin Chemistry Co., Ltd.), respectively. Then those two solutions were mixed and stirred for 12 hr at room temperature. The resulting solids were centrifuged and washed with ethanol three times and then dried at 110 °C overnight. UiO-66, MIL-96, HKUST-1, and MIL-101 were synthesized according to the methods reported previously (Cavka et al., 2008; Loiseau et al., 2006; Chui et al., 1999; Ferey et al., 2005).

1.2. Characterizations

The powder X-ray diffraction (XRD) patterns of all the samples were obtained using a D/max2550V apparatus (Rigaku, Japan) with Cu-Kα radiation source (λ=1.5406 Å), and its scanning angle of the samples was ranged from 5° to 75°. The N₂ adsorption-desorption isotherms and specific surface areas of the samples were measured by the Brunauer-Emmett-

Teller (BET) method with an apparatus (Micromeritics Tristar 3020 SIN 993, USA). An energy dispersive X-ray (EDX) spectrometer (Falcon 60S, USA) determined the sample's composition. The morphologies of the samples were observed by a scanning electron microscope (SEM, Hitachi S-3400N, Japan). A JEM-2100 Transmission Electron Microscopy (TEM) was used to observe the microscopic appearance and mapping images of the samples. The IR spectra of the samples was recorded using a Fourier transform infrared spectrometer (NICOLET iS10, USA) in transmittance mode, which was scanned in the region from 500 to 4000 cm^{-1} at a resolution of 1 cm^{-1} .

1.3. Mercury adsorption measurement

In this research, mercury chloride was chosen as the target pollutant and dissolved in deionized water to obtain test solutions of different Hg^{2+} concentrations. 10 mg of the MOFs powder was put into 20 mL of Hg^{2+} aqueous solution under stirring at ambient temperature. The concentration of Hg^{2+} and Co^{2+} in the initial solution and the filtrate after adsorption were determined by an Inductively Coupled Plasma Atomic Emission Spectrometer (ICP-OES Agilent 725, USA).

The mercury adsorption capacity (q_e) and removal efficiency (η) of the samples were determined by the following equations:

$$q_e = (C_0 - C_e) \times \frac{V}{m} \quad (1)$$

$$\eta = \frac{C_0 - C_e}{C_0} \times 100\% \quad (2)$$

Where C_0 (mg/L) and C_e (mg/L) were the initial and residual Hg^{2+} concentration, respectively. V (mL) was the volume of the solution, and m (mg) was the mass of the sample.

2. Results and discussion

2.1. Characterization of MOFs

Initial evidence of the as-synthesized MOFs samples was confirmed by powdered XRD. The powdered XRD patterns of the prepared UiO-66, MIL-96, HKUST-1, MIL-101 and ZIF-67 were shown in Fig. 1a. All as-synthesized samples were isostructural with the simulated ones, indicating the successful synthesis of MOFs. ZIF-67 showed narrow peaks, indicating its high crystallinity. After the treatment, the sample ZIF-67 that reached mercury adsorption saturation was also characterized by XRD. As illustrated in Fig. 1a, its XRD diffraction peaks were utterly different from those of fresh samples. The main diffraction peaks of the sample at 7.4° , 12.8° and 18.1° correspond to the (011), (112) and (222) lattices of the simulated ZIF-67. But the XRD diffraction peaks of ZIF-67 at 7.4° and 18.1° disappeared in the sample after adsorption. Therefore, it can be inferred that the crystal morphology of ZIF-67 changed after mercury adsorption. Fig. 1b–c showed the morphologies of ZIF-67 characterized by SEM and TEM. In the SEM image, it can be found that the obtained powder of ZIF-67 was consisted of crystals with regular and uniform polyhedral shapes and

smooth surface. The High-resolution TEM (inset of Fig. 1c) revealed the rhombic dodecahedron structure of ZIF-67 single crystal with an average particle size of approximately 290 nm. These ZIF-67 nanoparticles are porous due to the way MOFs are structured. This is a result of the geometry formed when metal ions and linkers arrange in an orderly manner forming pores (Singh et al., 2020). Fig. 1d showed the N_2 adsorption-desorption isotherm of the as-synthesized ZIF-67. It was a typical type-I curve, characteristic of microporous material. The BET specific surface area of ZIF-67 was 1146 m^2/g , which is huge. ZIF-67 has abundant channels and pores. The pore size distribution curve derived from N_2 desorption showed that ZIF-67 had peaks at 3.07 and 3.93 nm, but its pore size was mainly below 2 nm. It is a microporous material. Fig. 1e showed the Ball-and-stick model of ZIF-67 (Banerjee et al., 2008). It can be seen that the exhibited cavity of ZIF-67 was created by the connection of 2-methylimidazole molecules and cobalt tetrahedrons. Each cobalt ion is connected to four 2-methylimidazole molecules to build the three-dimensional structure of ZIF-67.

2.2. The Hg^{2+} adsorption performance of ZIF-67

UiO-66, MIL-96, HKUST-1, MIL-101, and ZIF-67 are MOFs with different organic ligands and metal ion nodes. 10 mg of each MOF samples were put into a 20 mL Hg^{2+} solution ($C_0 = 344$ mg/L, $\text{pH} = 4$) and then stirred 12 hr at room temperature to evaluate their Hg^{2+} removal performance. The best of them could only separate 9.56% of Hg^{2+} from water (Table 2). The Hg content adsorbed by these MOFs was very low ($\text{wt}\% < 0.16\%$), which is much lower than the core metal content of MOFs. In the meanwhile, ZIF-67 could remove 99.24% of Hg^{2+} from the aqueous solution and the Hg content of ZIF-67 after adsorption can reach 30%, which was much higher than the content of Co (12.91%). All of these MOFs are porous and have a huge specific surface area, but their Hg^{2+} removal performance was quite different, indicating that the rich pore structure is not the decisive factor in removing mercury ion with ZIF-67. The metal ion nodes of UiO-66, MIL-96, HKUST-1, and MIL-101 connected through carboxyl groups of organic ligands, but the cobalt ion nodes of ZIF-67 were through the nitrogen on the organic ligand. They built three-dimensional structures in different ways. This may be the reason why the Hg^{2+} removal efficiency of ZIF-67 is so different with other MOFs.

The pH of the solution always affected the performance of sorbents. In this study, the effect of pH on the sorption of Hg^{2+} by ZIF-67 was studied in the pH range of 2 to 6. The pH of the solution was adjusted by the addition of HCl and NaOH and the initial Hg^{2+} concentration of the solution was 510 mg/L. As shown in Fig. 2a, ZIF-67 exhibited low removal efficiency when treating Hg^{2+} solution with high acidity ($\text{pH} \leq 2$) due to its unstable structure in a strong acid environment (Howarth et al., 2016). When the pH value of the solution increased, the deprotonation effect on the surface of the sorbent promoted the adsorption of mercury ions (Luo et al., 2015). The Hg^{2+} removal performance of ZIF-67 was improved significantly, and the sample displayed high mercury removal efficiency in the pH range of 3 to 6. When the pH of the solution was greater than 4, the Hg^{2+} removal efficiency of ZIF-67 could be main-

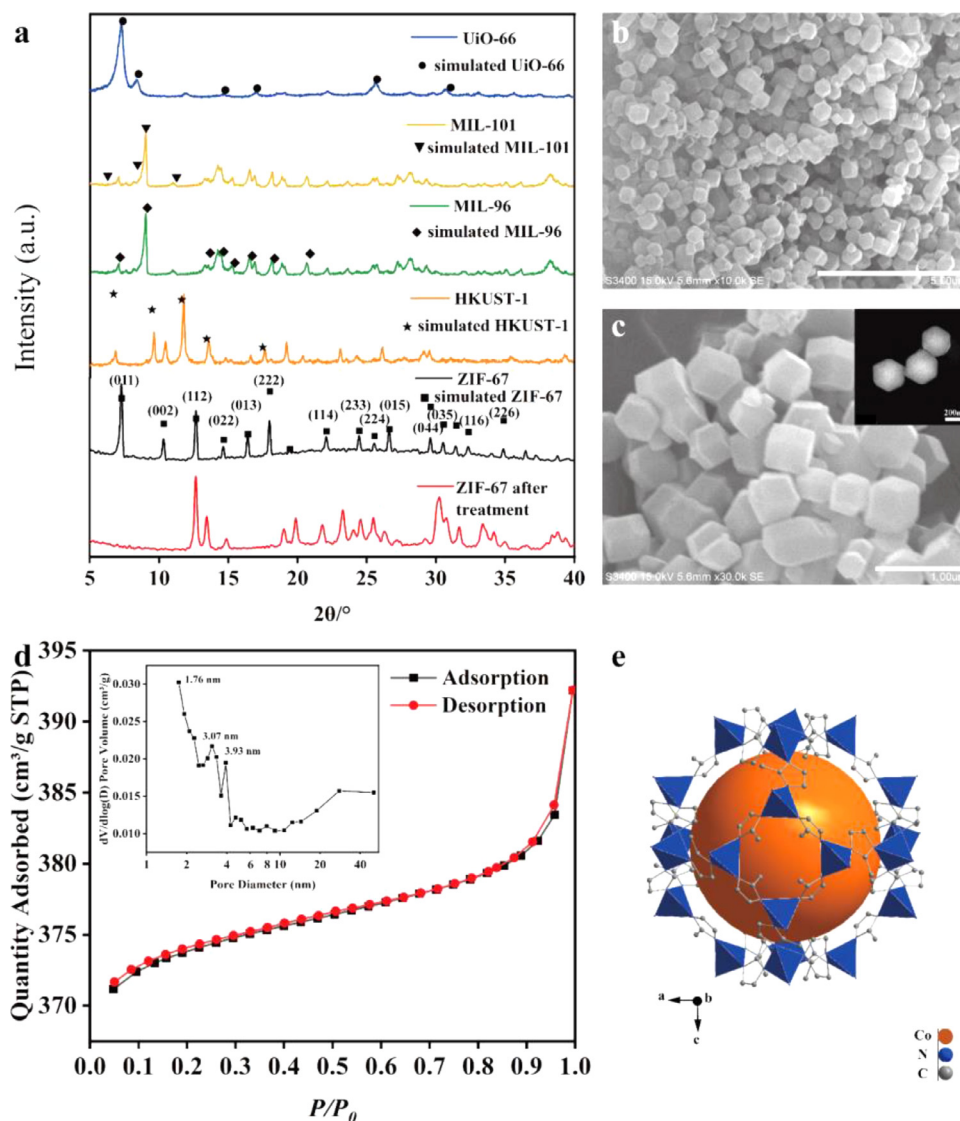


Fig. 1 – (a) powdered XRD patterns of as-synthesized and simulated MOFs, and ZIF-67 after Hg²⁺ adsorption; (b-c) SEM images of ZIF-67; inset shows the TEM image; (d) N₂ adsorption-desorption isotherms of ZIF-67; inset shows the pore size distribution of the sample; (e) schematic structure of ZIF-67 and its cavity.

tained at about 97%. Accordingly, pH=4 was chosen as the most suitable condition for the subsequent experiments.

The as-synthesized ZIF-67 (10 mg) was placed in a batch of HgCl₂ aqueous solution (20 mL) with different concentrations (1200, 1080, 768, 510, 344, 144, 64, 26, 7 mg/L) to further investigate its ability to remove mercury ion from aqueous solution. Fig. 2b showed the equilibrium Hg²⁺ sorption amount of the sample at different initial Hg²⁺ concentrations. ZIF-67 could remove 98.40% of the mercury ions from water and almost reach its mercury adsorption saturation when the solution's initial Hg²⁺ concentration was as high as 768 mg/L. After that, as the Hg²⁺ concentration increased, the amount of mercury ions captured by the sample increased slowly, and the maximum mercury ion uptake of the sample could reach 1740 mg/g. Its Hg²⁺ removal capacity was huge, which is higher than the most currently known MOFs sorbents (Halder et al., 2017; Ke et al., 2011b).

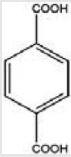
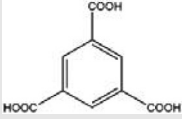
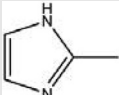


The Langmuir model describes an asymptotic approach to a specific maximum monolayer adsorption capacity, and the Freundlich model is applied to both monolayer and multilayer adsorption (Boparai et al., 2011; Tuzen et al., 2009; Yang et al., 2007). The Langmuir and Freundlich model equations can be expressed as follow:

$$\frac{C_e}{q_e} = \frac{1}{q_{\max}} K_L + \frac{C_e}{q_{\max}} \quad (3)$$

$$\ln q_e = \ln K_F + \frac{1}{n} \ln C_e \quad (4)$$

where q_{\max} (mg/g) is the maximum monolayer adsorption capacity, q_e (mg/g) is the amount of Hg²⁺ ions removed at equilibrium, C_e (mg/L) is the equilibrium concentration of Hg²⁺, and K_L is the Langmuir adsorption constant, K_F and n are the Freundlich adsorption constants.

Table 2 – The composition, parameters, and mercury removal performance of different MOFs.

Sorbents	Metal ion	Organic ligand	BET surface area (m ² /g)	Removal efficiency (%)	Metal content after adsorption (wt%)	
					Core metal	Hg
UiO-66	Zr ⁴⁺		700	9.56	26.03	0.06
MIL-101	Fe ³⁺		288	4.17	16.89	0.16
HKUST-1	Cu ²⁺		1089	5.81	31.04	0.04
MIL-96	Al ³⁺		366	2.91	9.76	0.03
ZIF-67	Co ²⁺		1146	99.24	12.91	30.01

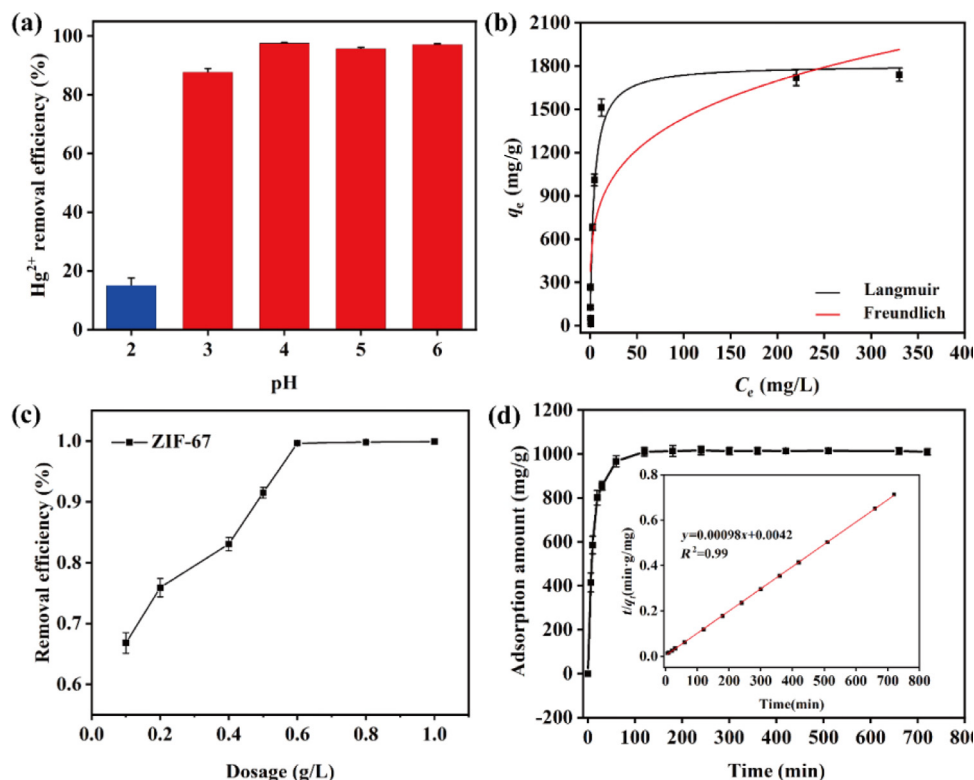


Fig. 2 – (a) The effect of pH on the adsorption of Hg²⁺ by ZIF-67; (b) Adsorption curve of Hg²⁺ at different Hg²⁺ concentrations by using the as-synthesized ZIF-67; (c) The effect of dosage on the adsorption of Hg²⁺ by ZIF-67 (initial Hg²⁺ concentration, $C_0 = 768$ mg/L); (d) Effect of contact time on the adsorption of Hg²⁺ to ZIF-67; inset shows the linear regression by fitting the experimental data with the pseudo-second-order model

According to Eqs. (3) and (4), the data in Fig. 2b were fitted using the Langmuir and Freundlich model, respectively. The results were shown in Appendix A Table S1. The correlation coefficient (R^2) value of the data fitting by the Langmuir isotherm was 0.97, much higher than that obtained by the Freundlich isotherm (0.77), indicating that the adsorption of Hg²⁺

onto ZIF-67 was monolayer adsorption. Meanwhile, the maximum Hg²⁺ adsorption capacity calculated by the Langmuir model was 1808 mg/g, slightly higher than the experimental value (1740 mg/g).

Fig. 2c showed the effect of dosage on the adsorption of Hg²⁺ by ZIF-67. As the dosage of ZIF-67 increased from 0.1 to

1.0 g/L, the Hg^{2+} removal efficiency increased from 66.80% to 99.90%. ZIF-67 could separate mercury ions from water efficiently with a dosage higher than 0.6 g/L even if the Hg^{2+} concentration of the solution was as high as 768 mg/L, showing its excellent Hg^{2+} removal performance.

2.3. Adsorption kinetics

In order to evaluate the adsorption properties of ZIF-67, the relationship between the contact time and the amount of Hg^{2+} sorbed by ZIF-67 was investigated. 10 mg of ZIF-67 was put into 20 mL of Hg^{2+} aqueous solution ($\text{pH} = 4$, $C_0 = 510 \text{ mg/L}$) and stirred for a set time (6, 10, 20, 30, 60, 120, 180, 240, 300, 360, 420, 510, 660, 720 min, respectively) at ambient temperature. As shown in Fig. 2d, ZIF-67 removed 99.00% of Hg^{2+} in the aqueous solution. It reached adsorption equilibrium within 120 min, suggesting that ZIF-67 also has a high adsorption efficiency in removing Hg^{2+} from water.

Different kinetic models (including the pseudo-first-order and pseudo-second-order) were used to match the experimental data to elucidate adsorption process's kinetics (Liu et al., 2019a).

$$\ln(q_e - q_t) = \ln q_e - k_1 t \quad (5)$$

$$\frac{t}{q_t} = \frac{1}{k_2 q_e^2} + \frac{t}{q_e} \quad (6)$$

where q_t (mg/g) is the adsorption amount of Hg^{2+} at time t . k_1 (min^{-1}) and k_2 ($\text{g} \cdot \text{mg}^{-1} \cdot \text{min}^{-1}$) are the pseudo-first-order and pseudo-second-order rate constants, respectively.

The fitted parameters obtained from kinetic models and their correlation coefficients (R^2) were shown in Appendix A Table S2. The matching degree between the kinetic data and the pseudo-first-order model was low ($R^2=0.71$), indicating this model's inapplicability to the current adsorption system. On the contrary, the pseudo-second-order model had a high correlation coefficient ($R^2=0.99$) with the experimental data. The linearity of its plot was shown in Fig. 2c, suggesting that the pseudo-second-order model could describe the adsorption of Hg^{2+} on ZIF-67.

2.4. Adsorption mechanism

The low Hg^{2+} removal performance of UiO-66, MIL-96, HKUST-1, and MIL-101 proved that it was inefficient to adsorb Hg^{2+} through the abundant pores of MOFs. Therefore, there must be another way for ZIF-67 to efficiently remove mercury ions. The treated solution was test by ICP-OES and it was found that when ZIF-67 removed mercury ions from the solution, an increase in the content of cobalt ions in the solution was also detected. Moreover, the amount of Co^{2+} in the final solution was observed to increase as the Hg^{2+} concentration of the initial solution increased, as shown in Fig. 3. Therefore, it was a reasonable inference that mercury ions left the solution by replacing the position of cobalt ions in ZIF-67. In the meanwhile, the amount of Hg^{2+} removed by the sample ZIF-67 has a linear relationship with that of cobalt ions entering the solution (inset of Fig. 2d). The curve slope was 0.127, which means that for every milligram of Hg^{2+} ions sorbed by the sample, 0.127 mg of cobalt ions in the ZIF-67 will be substituted and

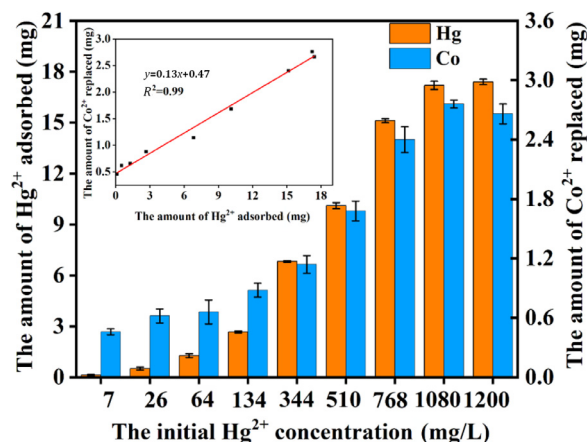


Fig. 3 – The amount of Hg^{2+} removed by the sample and the amount of Co^{2+} entering the solution changing with the initial Hg^{2+} concentration; inset shows the linear relationship between the amount of Hg^{2+} removed by the sample and the amount of Co^{2+} replaced from the sample.

entered into the solution. After calculation, the molar ratio of the Hg^{2+} ions removed by the sample to the Co^{2+} ions replaced was 2.31. This further confirms that the increase of cobalt ions in the solution is related to the decrease of mercury ions by the sample.

In this work, UV-vis was used to trace the solution after treatment, to confirm the release of organic ligand (mIM). The UV-vis method based on a standard curve could determine the mIM content in the solution accurately and rapidly. The standard curve of mIM was shown in Appendix A Fig. S1a. The correlation coefficient (R^2) value of the data was 0.995. Then 10 mg of ZIF-67 was put into deionized water and mercury-containing solution ($C_0=1080 \text{ mg/L}$). The change of mIM content in the solution over time was shown in Fig. 1Sb. When 10 mg of ZIF-67 was put into 20 mL of deionized water, mIM was continuously released into the water until its concentration reached about 0.49 g/L. However, when 10 mg of ZIF-67 was put into 20 mL of mercury-containing solution for 12 hr, the concentration of mIM in the solution reached 1.22 g/L. Therefore, it can be inferred that Hg^{2+} adsorbed onto the surface of ZIF-67 to snatch the mIM of Co^{2+} . This led to the destruction of the structure of MOFs, and a large amount of mIMs was released into the solution, making the concentration of mIM in the mercury-containing solution much higher than the mIM concentration released by ZIF-67 in deionized water.

Fig. 4a showed the color change of the sample powder after treatment as the initial Hg^{2+} concentration increased. It can be seen that the sample's color faded from purple to white as the Hg^{2+} concentration of the initial solution grew, which could be attributed to the reduction of cobalt ions in ZIF-67. The sample that had reached adsorption saturation was white, which is a useful feature of ZIF-67 that allows users to judge whether the sorbent is deactivated intuitively. As mentioned before, the powdered XRD pattern showed that the crystal morphology of ZIF-67 changed after mercury adsorption. The Field Emission Scanning electron microscope further revealed the changes in the microscopic morphology of the

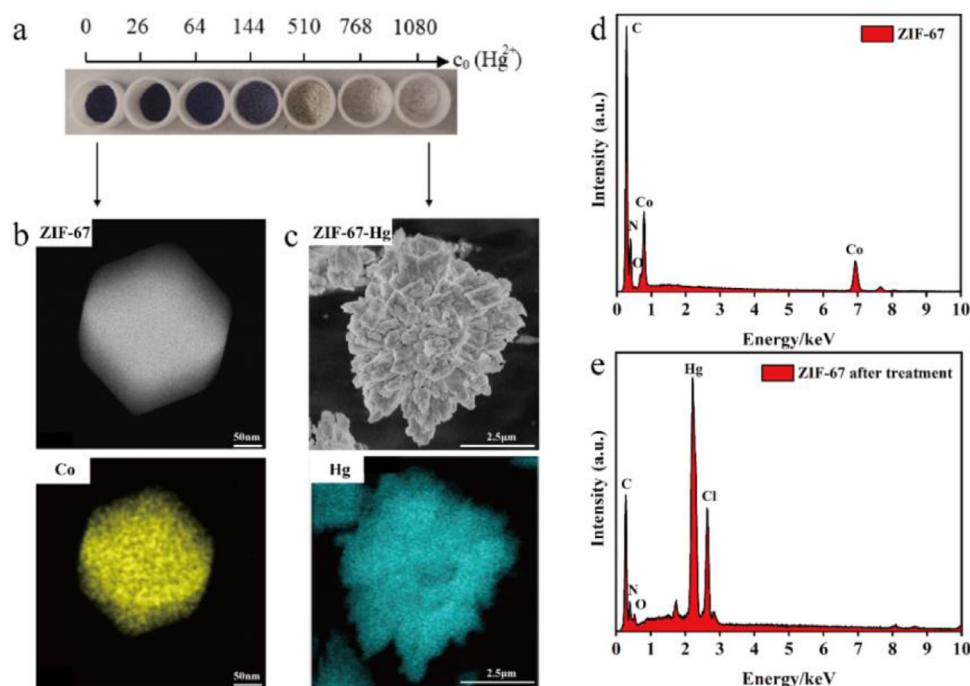


Fig. 4 – (a) The color change of sample powder after treatment as the initial Hg^{2+} concentration increased; (b-c) the FESEM and mapping images of ZIF-67 before and after treatment ($C_0 = 1080 \text{ mg/L}$); (d-e) the EDX spectra of ZIF-67 before and after treatment.

Table 3 – The element content of the sample before and after Hg^{2+} adsorption.

Sample	EDX result							Experimental data ^a	
	Content (At%)				Ratio ($n_a : n_b$)			$\text{Co}_{\text{rep}} : \text{Hg}_{\text{ads}}$	
	Co	N	Hg	Cl	N: Co	N: Hg	Hg: Co	$m_{\text{Co}} : m_{\text{Hg}}$	$n_{\text{Hg}} : n_{\text{Co}}$
ZIF-67	8.77	27.52	—	—	3.14	—	2.01	0.13	2.31
After adsorption	0	14.09	9.01	8.56	—	1.56	—	—	—

^a The experimental data was obtained from the linear relationship between the amount of Hg^{2+} removed by the sample and the amount of Co^{2+} replaced from the sample.

sample after treatment. Fig. 4b showed the FESEM image of fresh sample ZIF-67, and Fig. 4c showed that of the sample after treatment (the initial Hg^{2+} concentration, $C_0 = 1080 \text{ mg/L}$). The sample has reached adsorption saturation. The regular and uniform morphology of the fresh sample disappeared after encountering Hg^{2+} ions and turned into irregular flaky particles. In the meantime, the Mapping images of the samples revealed that ZIF-67 indeed captured Hg^{2+} in the aqueous solution, and the capture amount was very high. The EDX spectra of the sample before and after the treatment was shown in Fig. 4d-4e. In Fig. 4e, the main cobalt peaks were not observed, indicating that most of the cobalt in ZIF-67 has been replaced by a high content of mercury element after treatment.

Table 3 showed the contents of elements in the sample before and after the treatment with Hg^{2+} solution. Most of cobalt in ZIF-67 has been replaced by a high content of mercury element after treatment. The molar ratio of the removed mercury content to the replaced cobalt content in the samples before and after the treatment ($n_{\text{Hg}} : n_{\text{Co}}$) was 2.01, corresponding to

the previous experimental data (2.31). Therefore, it can be inferred that during the treatment, every two Hg^{2+} ions replaced one Co^{2+} ion in ZIF-67. Each cobalt ion node is connected to four mIMs through coordinate bonds in ZIF-67 (Li et al., 2016; Zhu et al., 2020), so it is a reasonable inference that Hg^{2+} had two coordinated bonds with mIMs in the sample after treatment.

The binding of mercury by imidazole is great that mercury ions can form a covalent bond with the nitrogen(3) on the imidazole ring with a lone pair of electrons (Brooks and Davidson, 1966; Mubark et al., 2020). According to the NIST Atomic Spectra Database, the ionization energy of Hg^{2+} (34.49 eV) is higher than that of Co^{2+} (33.50 eV), which means that with the same ligand, the coordination compound formed by Hg^{2+} is more stable than that formed by Co^{2+} . Thus, the phenomenon that Hg^{2+} replaced Co^{2+} in ZIF-67 can be attributed to the stronger coordination ability of Hg^{2+} with mIM than Co^{2+} .

The EDX results also showed that chlorine appeared in the sample after treatment and its content (At%) was similar to

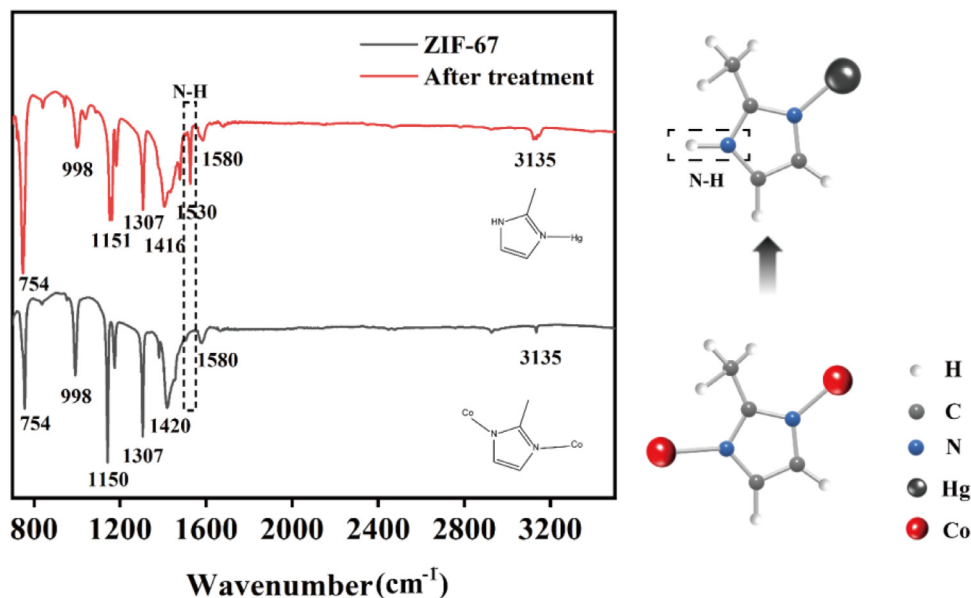
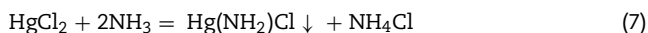


Fig. 5 – The FT-IR spectra and Kekule models of ZIF-67 before and after treatment.

that of mercury. The ammoniating of mercuric chloride can produce precipitation $\text{Hg}(\text{NH}_2)\text{Cl}$, and its process can be described as Eq. (7). The ratio of mercury and chloride is 1:1, and Hg^{2+} has two coordination with NH_2 in $\text{Hg}(\text{NH}_2)\text{Cl}$, which was similar to the sample after treatment in this work.



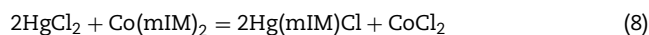
To relate the excellent Hg^{2+} removal performance with the MOF structure, the FT-IR spectra of ZIF-67 before and after treatment was obtained, as shown in Fig. 5. The peaks in the range of $754\text{--}1580\text{ cm}^{-1}$ were associated with the stretching and bending modes of the mIM (Wang et al., 2020). The convoluted peaks at $1307\text{--}1500\text{ cm}^{-1}$ were attributed to the entire ring stretching (Ammar et al., 2016). The stretching vibrations of the $\text{C}=\text{N}$ bonding appeared at 1580 cm^{-1} (Hou and Wu, 2020). All the peaks of the sample after treatment agreed well with those of the fresh sample, except for the peak at 1530 cm^{-1} that can be attributed to the N-H bending (Zhang et al., 2013). The sample ZIF-67 after treatment had a N-H bending peak which did not appear in the fresh sample. In the structure of IM, there are two nitrogen atoms on the imidazole ring. The nitrogen(1) has a N-H bond with the hydrogen atom, but the nitrogen(3) does not. This means when Hg^{2+} replaced the position of cobalt ion in ZIF-67, it did not formed bonds with all the nitrogen of mIMs. During the treatment, it destroyed the 3D structure of ZIF-67 built by cobalt ions and mIMs. But unlike Co^{2+} , it only coordinated with nitrogen(3) on the imidazole ring of mIMs, not with nitrogen(1), resulting in the appearance of the strong N-H peak in the FT-IR spectra. The different coordination methods between Co^{2+} and Hg^{2+} resulted in changes in morphology of ZIF-67 after the treatment. This also explains why the molar ratio between the cobalt ions entering the solution and the removed mercury ions is about 2. When a cobalt ion disconnected from four IMs, two nitrogen(3) of IM are exposed in the solution. Then two mercury ions re-

placed the position of the cobalt ion and formed bonds with these nitrogen(3).

Since the coordination number of Hg^{2+} is 2, Hg^{2+} cannot build a three-dimensional pore structure with mIMs like Co^{2+} , which can be proved by the N_2 adsorption and desorption isotherm of ZIF-67-Hg. The N_2 adsorption-desorption isotherm of ZIF-67-Hg conformed to the IV curve, which often appears in the multi-layer adsorption process of mesoporous materials. The BET specific surface area of ZIF-67-Hg was $18.6\text{ m}^2/\text{g}$, which was much smaller than that of ZIF-67 ($1146\text{ m}^2/\text{g}$). ZIF-67 had a large number of micropores (pore size $< 2\text{ nm}$). However, the pore size distribution diagram of ZIF-67-Hg showed that the pore size of the sample after adsorption was mainly about 20 nm . ZIF-67-Hg was a mesoporous material. Its structure was completely different from ZIF-67. The SEM image of ZIF-67-Hg (Fig. 6b) showed that its morphology was flaky particles, completely different from ZIF-67.

After adsorption, the chemical state of the sample also changed. The pH stability of ZIF-67 and ZIF-67-Hg was tested, as shown in Fig. 6c. When the pH of the solution is less than 2, neither ZIF-67 nor ZIF-67-Hg can exist stably. When the pH is greater than 3, the weight loss rate of ZIF-67-Hg is less than that of ZIF-67, which shows that the chemical stability of ZIF-67-Hg is higher than that of ZIF-67.

The mechanism of ZIF-67's high-efficiency mercury removal performance is clear. It can be confirmed that mercury ions replaced the position of the cobalt ion in ZIF-67 and form coordinate bonds with the nitrogen(3) on the ring of mIM to achieve the separation of mercury ions during the treatment, as shown in Fig. 7. Its process can be described as Eq. (8).



In summary, mIMs is the reaction center of ZIF-67, which can efficiently separate Hg^{2+} from the solution. Therefore, adding mIMs to the solution directly can also remove Hg^{2+} .

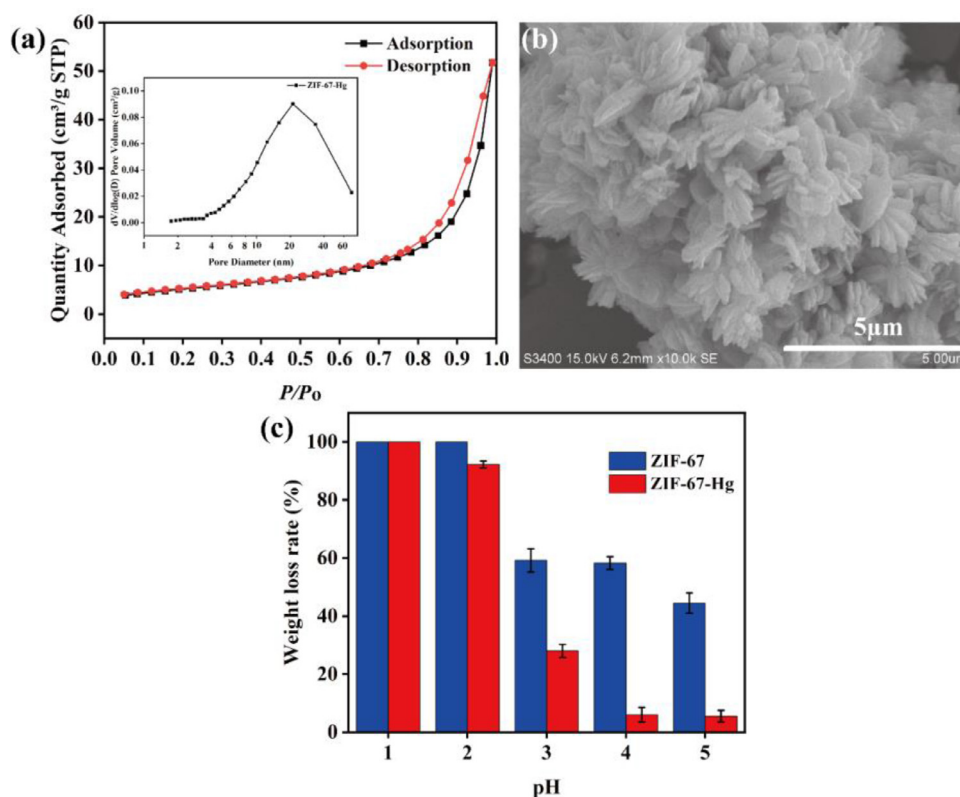


Fig. 6 – (a) N_2 adsorption-desorption isotherms of ZIF-67-Hg; inset shows the pore size distribution of the sample; (b) The SEM image of ZIF-67-Hg; (c) The weight loss rate of ZIF-67 and ZIF-67-Hg after being putting into solutions with different pH values for 6 hr.

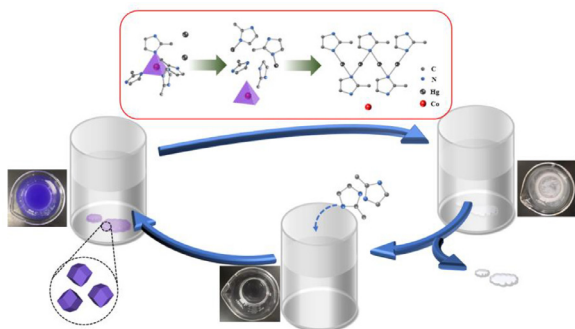


Fig. 7 – The mechanism diagram of Hg^{2+} removal using ZIF-67 and its regeneration.

However, it is not efficient to directly use mIMs to removal Hg^{2+} . mIM is easily soluble in water and it is difficult to recycle, so its utilization rate is not high when using it to treat low-concentration Hg^{2+} solution. At the same time, it is difficult to judge whether the mercury ions in the solution are completely removed. In order to ensure that the reaction is complete, it is necessary to add an excessive amount of mIMs. ZIF-67 has good hydrothermal stability. It can fix mIMs in water and release mIMs only when it encounters Hg^{2+} , making the utilization rate of mIMs higher. At the same time, ZIF-67 can display the remaining amount of effective mIMs in its struc-

ture through color changes. If the sample does not turn white after treating the solution, it means the effective mIMs has not been used up and Hg^{2+} in the treated solution has been completely removed. ZIF-67 can effectively improve the utilization of mIM.

2.5. Recycling of ZIF-67

ZIF-67 was synthesized simply by stirring the reactants at room temperature, so it could be recycled by adding organic ligands (mIMs) to the solution after treatment, as shown in Fig. 7. The substituted cobalt ions in the solution reacted with mIMs to regenerate ZIF-67. The reaction was quick. When mIMs was added to the treated solution, the solution immediately turns purple due to the formation of ZIF-67. This process not only regenerated ZIF-67, but also recovered cobalt ions in the treated solution.

2.6. Selectivity toward metal ions

The selective adsorption of Cu^{2+} , Zn^{2+} , Ag^+ , Pb^{2+} and Hg^{2+} by ZIF-67 from the solution was studied. 10 mg of ZIF-67 was put into 20 mL of a solution containing a mixture of all of the five ions with the initial concentrations of 100 mg/L. The solution after stirring for 1 hr was tested for metal content by ICP-OES. The affinity of ZIF-67 toward these metal ions can be expressed in terms of the distribution coefficient (K_d). K_d was

Table 4 – Adsorption of ZIF-67 toward the mixed ions.

Metal ions	C ₀ (mg/L)	C _{t-1h} (mg/L)	Removal (%)	K _d (mL/g)
Cu	100.0	9.1	90.9	2.0 × 10 ⁴
Zn	100.0	65	35	1.1 × 10 ³
Hg	100.0	8.0	92.0	2.3 × 10 ⁴
Pb	100.0	6.4	93.6	2.9 × 10 ⁴
Ag	100.0	85.7	14.2	3.3 × 10 ²
V=20 mL		m=10 mg		time= 60 min

calculated according to Eq. (9):

$$K_d = \frac{(C_0 - C_t) V}{C_t \times m} \times 10^3 \quad (9)$$

where C₀ (mg/L) and C_t (mg/L) are the initial metal ions concentration and the metal ions concentration at time t, m (mg) is the mass of the adsorbent and V (mL) is the volume of the adsorbate solution.

In general, K_d values above 10⁴ mL/g are considered to be exceptional sorbents (Fard et al., 2015). The obtained K_d values of ZIF-67 toward mixed metal ions are given in Table 4. It can be seen that the selectivity order for these metal ions was: Pb²⁺ > Hg²⁺ > Cu²⁺ > Zn²⁺ > Ag⁺. The selectivity toward Hg²⁺, Pb²⁺, and Cu²⁺ is much higher than Zn²⁺ and Ag⁺. Therefore, ZIF-67 is effective in the selective adsorption of Hg²⁺, Pb²⁺, and Cu²⁺.

3. Conclusions

In this work, a new strategy was applied to MOFs material to separate mercury ions from wastewater, which utilizes the stronger coordination ability of Hg²⁺ with the organic ligands than the metal ion nodes in MOFs. ZIF-67 executed this strategy well and exhibited a huge Hg²⁺ adsorption capacity of 1740 mg/g. It has abundant mIMs as organic ligands, which can coordinate with mercury ions through the nitrogen(3) on its imidazole ring. mIMs is the reaction center and ZIF-67 can improve its utilization effectively. ZIF-67 is also high-efficient that it can remove 99% of Hg²⁺ in the aqueous solution within 120 min. Its adsorption data agreed well with the Langmuir model and pseudo-second-order model. It can be sustainable recycled by adding organic ligands to the solution after treatment due to its simple synthesis method at room temperature. It's a high-efficient and sustainable sorbent for Hg²⁺ removal from wastewater.

Acknowledgments

This work was supported by the National Natural Science Foundation of China (Nos. 51778229, 21307032) and the Fundamental Research Funds for the Central Universities (No. JKB012015019).

Appendix A Supplementary data

Supplementary material associated with this article can be found, in the online version, at doi:10.1016/j.jes.2021.08.032.

REFERENCES

- Ammar, M., Jiang, S., Ji, S., 2016. Heteropoly acid encapsulated into zeolite imidazolate framework (ZIF-67) cage as an efficient heterogeneous catalyst for Friedel-Crafts acylation. *J. Solid State Chem.* 233, 303–310.
- Babic, B.M., Milonjic, S.K., Polovina, M.J., Cupic, S., Kaludjerovic, B.V., 2002. Adsorption of zinc, cadmium and mercury ions from aqueous solutions on an activated carbon cloth. *Carbon* 40, 1109–1115.
- Banerjee, R., Phan, A., Wang, B., Knobler, C., Furukawa, H., O'Keeffe, M., et al., 2008. High-throughput synthesis of zeolitic imidazolate frameworks and application to CO₂ capture. *Science* 319, 939–943.
- Bhattacharjee, S., Lee, Y.R., Ahn, W.S., 2015. Post-synthesis functionalization of a zeolitic imidazolate structure ZIF-90: a study on removal of Hg(II) from water and epoxidation of alkenes. *Crystengcomm* 17, 2575–2582.
- Boparai, H.K., Joseph, M., O'Carroll, D.M., 2011. Kinetics and thermodynamics of cadmium ion removal by adsorption onto nano zerovalent iron particles. *J. Hazard. Mater.* 186, 458–465.
- Brooks, P., Davidson, N., 1966. Mercury(II) Complexes of Imidazole and Histidine. *J. Am. Chem. Soc.* 82, 2118–2123.
- Choi, J.M., Jeong, D., Cho, E., Jun, B.H., Park, S., Yu, J.H., et al., 2016. Chemically functionalized silica gel with alkynyl terminated monolayers as an efficient new material for removal of mercury ions from water. *J. Ind. Eng. Chem.* 35, 376–382.
- Fard, Z.H., Malliakas, C.D., Mertz, J.L., Kanatzidis, M.G., 2015. Direct extraction of Ag⁺ and Hg²⁺ from cyanide complexes and mode of binding by the layered K₂MgSn₂S₆ (KMS-2). *Chem. Mater.* 27, 1925–1928.
- Halder, S., Mondal, J., Ortega-Castro, J.N., Frontera, A., Roy, P., 2017. A Ni-based MOF for selective detection and removal of Hg²⁺ in aqueous medium: a facile strategy. *Dalton T* 46, 1943–1950.
- Hou, B., Wu, J., 2020. Halloysite nanotubes (HNTs)@ZIF-67 composites-a new type of heterogeneous catalyst for the Knoevenagel condensation reaction. *Dalton Trans.* (Cambridge, England: 2003) 49, 17621–17628.
- Howarth, A.J., Liu, Y., Li, P., Li, Z., Wang, T.C., Hupp, J., et al., 2016. Chemical, thermal and mechanical stabilities of metal-organic frameworks. *Nature Rev. Mater.* 1, 15018.
- Jeon, C., Park, K.H., 2005. Adsorption and desorption characteristics of mercury(II) ions using aminated chitosan bead. *Water Res.* 39, 3938–3944.
- Ke, F., Qiu, L.G., Yuan, Y.P., Peng, F.M., Jiang, X., Xie, A.J., Shen, Y.H., Zhu, J.F., 2011b. Thiol-functionalization of metal-organic framework by a facile coordination-based postsynthetic strategy and enhanced removal of Hg²⁺ from water. *J. Hazard. Mater.* 196, 36–43.
- Krishnan, K.A., Anirudhan, T.S., 2002. Removal of mercury(II) from aqueous solutions and chlor-alkali industry effluent by steam activated and sulphurised activated carbons prepared from bagasse pith: kinetics and equilibrium studies. *J. Hazard. Mater.* 92, 161–183.
- Li, L., Feng, Y., Qiu, Y.R., Li, Y.S., Wu, K.Y., Zhu, L.D., 2020. A three-dimensional bimetallic oxide NiCo₂O₄ derived from ZIF-67 with a cage-like morphology as an electrochemical platform for Hg²⁺ detection. *Microchem. J.* 155, 9.
- Li, S., Peng, S., Huang, L., Cui, X., Al-Enizi, A.M., Zheng, G., 2016. Carbon-coated Co³⁺-rich cobalt selenide derived from ZIF-67

- for efficient electrochemical water oxidation. *Acs Appl. Mater. Inter.* 8, 20534–20539.
- Liang, L., Chen, Q., Jiang, F., Yuan, D., Qian, J., Lv, G., et al., 2016. In situ large-scale construction of sulfur-functionalized metal-organic framework and its efficient removal of Hg(II) from water. *J. Mater. Chem. A* 4, 15370–15374.
- Liu, C., Peng, J., Zhang, L., Wang, S., Ju, S., Liu, C., 2018. Mercury adsorption from aqueous solution by regenerated activated carbon produced from depleted mercury-containing catalyst by microwave-assisted decontamination. *J. Clean Prod.* 196, 109–121.
- Liu, C., Zeng, S., Yang, B., Jia, F., Song, S., 2019a. Simultaneous removal of Hg^{2+} , Pb^{2+} and Cd^{2+} from aqueous solutions on multifunctional MoS_2 . *J. Mol. Liq.* 296, 109–121.
- Liu, F., Xiong, W., Feng, X., Shi, L., Chen, D., Zhang, Y., 2019b. A novel monolith ZnS-ZIF-8 adsorption material for ultraeffective Hg (II) capture from wastewater. *J. Hazard. Mater.* 367, 381–389.
- Luo, F., Chen, J.L., Dang, L.L., Zhou, W.N., Lin, H.L., Li, J.Q., et al., 2015. High-performance Hg^{2+} removal from ultra-low-concentration aqueous solution using both acylamide- and hydroxyl-functionalized metal-organic framework. *J. Mater. Chem. A* 3, 9616–9620.
- Matlock, M.M., Henke, K.R., Atwood, D.A., Robertson, D., 2001. Aqueous leaching properties and environmental implications of cadmium, lead and zinc trimercaptotriazine (TMT) compounds. *Water Res.* 35, 3649–3655.
- Mubark, H.M.H., Witwit, I.N., Ali, A.A.M., 2020. Synthesis of new azo imidazole ligand and fabricating its chelate complexes with some metallic ions. *J. Phys.* 1660 (012031) (012039 pp.)-012031 (012039 pp.).
- Olson, E.S., Miller, S.J., Sharma, R.K., Dunham, G.E., Benson, S.A., 2000. Catalytic effects of carbon sorbents for mercury capture. *J. Hazard. Mater.* 74, 61–79.
- Park, K.S., Ni, Z., Cote, A.P., Choi, J.Y., Huang, R., Uribe-Romo, F.J., et al., 2006. Exceptional chemical and thermal stability of zeolitic imidazolate frameworks. *P. Natl. Acad. Sci. U.S.A.* 103, 10186–10191.
- Ramezani, M.S., Ozdemir, J., Khosropour, A.R., Beyzavi, M.H., 2020. Sulfur-decorated hyper-cross-linked coal tar: a microporous organic polymer for efficient and expeditious mercury removal. *Acs Appl. Mater. Inter.* 12, 44117–44124.
- Saleem, H., Rafique, U., Davies, R.P., 2016. Investigations on post-synthetically modified UiO-66- NH_2 for the adsorptive removal of heavy metal ions from aqueous solution. *Micropor. Mesopor. Mat.* 221, 238–244.
- Singh, S., Numan, A., Zhan, Y., Singh, V., Tran Van, H., Nguyen Dang, N., 2020. A novel highly efficient and ultrasensitive electrochemical detection of toxic mercury (II) ions in canned tuna fish and tap water based on a copper metal-organic framework. *J. Hazard. Mater.* 399.
- Song, B.Y., Eom, Y., Lee, T.G., 2011. Removal and recovery of mercury from aqueous solution using magnetic silica nanocomposites. *Appl. Surf. Sci.* 257, 4754–4759.
- Tuzen, M., Sari, A., Mendil, D., Soylak, M., 2009. Biosorptive removal of mercury(II) from aqueous solution using lichen (*Xanthoparmelia conspersa*) biomass: Kinetic and equilibrium studies. *J. Hazard. Mater.* 169, 263–270.
- Wang, C., Tao, S., Wei, W., Meng, C., Liu, F., Han, M., 2010. Multifunctional mesoporous material for detection, adsorption and removal of Hg^{2+} in aqueous solution. *J. Mater. Chem.* 20, 4635–4641.
- Wang, Q., Sun, W., Xie, T.Y., Cao, L.M., Yang, J., 2019. Metal-organic framework (MOF) template based efficient Pt/ZrO₂@C catalysts for selective catalytic reduction of H₂ below 90 degrees C. *Chem.-Asian J.* 14, 416–421.
- Wang, Z., Ren, D., Yu, H., Jiang, S., Zhang, S., Zhang, X., 2020. Study on improving the stability of adsorption-encapsulation immobilized Laccase@ZIF-67. *Biotechnol. Reports (Amsterdam, Netherlands)* 28, e00553.
- Xia, M.D., Chen, Z.X., Li, Y., Li, C.H., Ahmad, N.M., Cheema, W.A., et al., 2019. Removal of Hg(II) in aqueous solutions through physical and chemical adsorption principles. *Rsc. Adv.* 9, 20941–20953.
- Xiong, C., Wang, S., Zhang, L., Li, Y., Srinivasakannan, C., Peng, J., 2018. Preparation and application of phosphinic acid functionalized nanosilica for the effective removal of mercury (II) in aqueous solutions. *J. Sol-Gel Sci. Technol.* 87, 442–454.
- Yang, J., Peng, J., Jia, J., Fang, H., 2007. Adsorption of carbon disulfide (CS_2) in water by different types of activated carbon-equilibrium, dynamics, and mathematical modeling. *J. Environ. Eng.-Asce.* 133, 294–302.
- Yee, K.K., Reimer, N., Liu, J., Cheng, S.Y., Yiu, S.M., Weber, J., et al., 2013. Effective mercury sorption by thiol-laced metal-organic frameworks: in strong acid and the vapor phase. *J. Am. Chem. Soc.* 135, 7795–7798.
- Zabihi, M., Asl, A.H., Ahmadpour, A., 2010. Studies on adsorption of mercury from aqueous solution on activated carbons prepared from walnut shell. *J. Hazard. Mater.* 174, 251–256.
- Zhang, F.S., Nriagu, J.O., Itoh, H., 2005. Mercury removal from water using activated carbons derived from organic sewage sludge. *Water Res.* 39, 389–395.
- Zhang, Z.P., Rong, M.Z., Zhang, M.Q., Yuan, C., 2013. Alkoxyamine with reduced homolysis temperature and its application in repeated autonomous self-healing of stiff polymers. *Polymer Chem.* 4, 4648–4654.
- Zhao, X., Wang, Y.X., Li, D.S., Bu, X.H., Feng, P.Y., 2018. Metal-organic frameworks for separation. *Adv. Mater.* 30, 34.
- Zhu, R., Ding, J., Yang, J., Pang, H., Xu, Q., Zhang, D., Braunstein, P., 2020. Quasi-ZIF-67 for boosted oxygen evolution reaction catalytic activity via a low temperature calcination. *Acs Appl. Mater. Inter.* 12, 25037–25041.
- Zou, F., Yu, R., Li, R., Li, W., 2013. Microwave-assisted synthesis of HKUST-1 and functionalized HKUST-1-@H₃PW₁₂O₄₀: selective adsorption of heavy metal ions in water analyzed with synchrotron radiation. *Chem. Phys. Chem.* 14, 2825–2832.